IEEE Access
Multidisciplinary | Rapid Review | Open Access Journal

Received 20 March 2024, accepted 5 April 2024, date of publication 12 April 2024, date of current version 22 April 2024.

*Digital Object Identifier 10.1109/ACCESS.2024.3387944*

RESEARCH ARTICLE

# Differential Evolution-Based Sample Consensus Algorithm for the Matching of Remote Sensing Optical Images With Affine Geometric Differences

**SOURABH PAUL[1], RAVI TIWARI[1], AMIT KUMAR RAHUL[2], MANOJ KUMAR SINGH[2], AND PRATHAM GUPTA[3]**

[1]School of Electronics Engineering (SENSE), Vellore Institute of Technology (VIT), Chennai, Tamil Nadu 600127, India
[2]Division of Mathematics, School of Advance Sciences (SAS), Vellore Institute of Technology (VIT), Chennai, Tamil Nadu 600127, India
[3]School of Computer Science and Engineering (SCOPE), Vellore Institute of Technology (VIT), Chennai, Tamil Nadu 600127, India

Corresponding author: Sourabh Paul (sourabh.paul@vit.ac.in)

This work was supported by the Vellore Institute of Technology (VIT), Chennai Campus, Chennai, India.

**ABSTRACT** Optical image matching has been a recent trend in the field of remote sensing image processing. It is considered as a challenging problem due to the existence of significant geometric variations as well as intensity differences between the images. Scale invariant feature transform (SIFT) is one of the most effective schemes to handle these factors. However, it produces many false matches in the matching of the remote sensing images which effect its performance. In order to address this issue, a novel Differential Evolution-based Sample Consensus Algorithm (DESCA) is proposed to eliminate these false matches and retain the correct matches. The proposed DESCA scheme is very effective for the images having significant affine geometric differences. It has the ability to provide more correct matches. Several sets of remote sensing optical image pairs are used to test the performance of the proposed method. It obtains the Root Mean Square Error (RMSE) value in the range of 0.67 to 0.95 pixels which indicates that the sub-pixel accuracy is achieved. The experimental results show that the proposed method provides more correct matching pairs and better mutual information (MI) values than the state-of-the-art methods.

**INDEX TERMS** Scale-invariant feature transform (SIFT), differential evolution (DE), sample consensus algorithm (SCA).

## I. INTRODUCTION

Image matching is defined as the technique of obtaining correct correspondences between the images of the same scene [1]. It has been utilized as one of the main important steps in many remote sensing applications such as change detection, border monitoring, urban monitoring and image fusion. Over the last few years, a variety of algorithms have been developed for the matching of remote sensing optical images. However, most of the algorithms produce many outliers in the matching process which effects their performance. The elimination of these outliers is still a critical issue for the optical images having significant affine geometric differences.

Over the last few decades, the availability and volume of the remote sensing optical images have been improved tremendously [2]. In [3], a freely available benchmark data set was provided for different remote sensing applications such as cross-city semantic segmentation. The hyperspectral and mutispectral images obtained by different remote sensing sensors have been utilized in many fields [4]. The image matching is considered as one of the primary steps in various remote sensing applications. Optical image matching can be performed in two different ways: intensity-based methods and feature-based methods. The intensity-based methods perform the matching between the input images by using

The associate editor coordinating the review of this manuscript and approving it for publication was Zhan-Li Sun.

a similarity metric such as cross-correlation and mutual information. These methods generally use an optimization technique to find the registration peak in less computational time [5]. The feature-based methods follow feature extraction and matching operations in image matching. These are more effective to handle significant geometric and intensity differences between the optical images than the intensity-based methods.

Scale-invariant feature transform (SIFT) [6] is a widely used feature-based method for the matching of the remote sensing optical images. However, it suffers from uneven distribution of extracted features and a lack of controllability over them. In order to resolve these issues, its improved versions uniform robust SIFT (UR-SIFT) [1] and Modified UR-SIFT (M-UR-SIFT) [7] are developed. Over the years various enhanced versions of the SIFT algorithm have been developed to further improve its performance. In [8], a multilevel SIFT-based scheme is developed to match the remote sensing images by representing them at different resolution levels. This method can increase the number of matching pairs. In [9], a SIFT-based adaptive block processing method is implemented to improve its matching performance. This method significantly improves the distribution quality of the extracted features. In [10], an adaptive Redundant keypoint elimination method (A-RKEM) is developed based on SIFT to eliminate the redundant SIFT features. In [11], distinctive order based self-similarity descriptor is developed along with the UR-SIFT algorithm to match the optical images. This method is very much effective the handle the nonlinear intensity differences. Ye et al. [12] developed an optical image matching algorithm using an enhanced version of SIFT along with local self-similarity descriptor [13]. This methods provides better position accuracy in matching. In [14], the corner and blob features are extracted from the input images and SIFT descriptor is constructed for each of the features. Jiang et al. [15] developed a matching algorithm based on SIFT, shape context, and local structure constraint. Moreover, in [16], SIFT features are used along with the corner features to provide evenly distributed matching pairs in image matching. In this method, two types of features are matched separately and correct matches are identified. Other than the SIFT algorithm, some other image matching algorithms can be found in the literature. Speeded-up robust feature (SURF) [17] and Oriented FAST and rotated BRIEF (ORB) [18] are another two widely used schemes to match the remote sensing images. In [19], a multichannel autocorrelation of the log-Gabor-based feature detector is presented to match remote sensing images. Zhou et al. [20] utilized the multiscale convolutional gradient features to match optical and synthetic aperture radar (SAR) images. In [21], an image matching algorithm is developed using steerable filters and fast cross-correlation-based similarity measure. These methods provide better position accuracy in remote sensing image matching.

Outlier elimination is considered as a challenging problem in optical image matching, especially for the images having affine geometric differences. It is a well-known fact that the effectiveness of a matching algorithm is highly affected by the existence of outliers in the set of matching pairs. A variety of SIFT-based schemes have been developed in recent time to eliminate the outliers from the matching pairs. Dual matching (DM) [22] is one of them where the outliers are eliminated by finding the nearest neighbor distance ratio (NNDR) for both the input image features. Random sample consensus (RANSAC) [23] is one of the well-known schemes to remove the outliers in matching pairs. However, it takes significant computational time when too many outliers exit in the matching pairs. Wu et al. proposed a fast sample consensus (FSC) [24] algorithm to eliminate the false matches. This algorithm is based on the idea of RANSAC and it is developed to increase the number of correct matches in less computational time. In [25], the outliers are removed by using the dominant orientation consistency (DOC) property of the SIFT features. In this method, an orientation histogram is constructed by using the dominant orientation deflection of the corresponding features. Kupfer et al. [26] utilized the orientation and scale information of the standard SIFT features to eliminate the mismatches. This method can increase the number of correct matches in image matching. In [27], a miss-match elimination method is proposed based on maximum gradient and edge orientation (MGEO). This method can give better position accuracy in image matching. In [28], Paul et al. presented an outlier removal scheme by estimating the scale and orientation differences between the input images using the matching candidates. This method is very effective to provide more correct matching pairs. Ma et al. [29] utilized the scale, orientation, and translation differences between the matching pairs to eliminate the outliers. However, most of these algorithms are developed for the images with similarity transformation differences. Many of them can not be applied for the optical images having affine geometric differences. In [30], a particle swarm optimization sample consensus algorithm (PSOSAC) is proposed to remove the outliers for the images with affine geometric differences. This method combines the idea of RANSAC with the PSO. However, the performance of the differential evolution (DE) algorithm is largely better than the PSO [31]. In addition, initialization of the PSO parameters for the identification of correct matches is a critical task.

DE Optimization is one of the highly effective stochastic real-parameter optimization schemes. The main objective of this optimization is to update a $D$ dimensional vector $X = [x_1, x_2, x_3, .., x_D]$ until the objective function $f(X)$ provides the best result (minimum or maximum value). The main advantage of the DE optimization is that it uses less number of control parameters ($C_r$ and $F$) in the optimization process. It contains four steps: initialization, difference vector mutation, crossover, and selection. The parameter $F$ is a scalar factor which is used to update a donor vector in the mutation step whereas, $C_r$ plays an important role in

generating a trail vector in the crossover step. In [31], a detailed review of the different DE optimization techniques was presented. The DE optimization has been widely applied in several domains such as classification problems, industrial control, wireless sensor network, computational systems, and image segmentation [32]. In [33], a binary DE algorithm was developed to improve the classification performance by selecting appropriate features. In [34], the electric, mechanical, and magnetic subsystem parameters of a line-start interior permanent magnet synchronous motor are simultaneously identified using a differential-evolution (DE)-based technique. In [35], a multi-objective differential evolution algorithm was implemented to simultaneously optimize the sensor distribution over different area shapes, expand the coverage area and lower the network energy. In [36], the calibration of the computational neuroscience model was performed by using DE. In [37], the DE algorithm was utilized to perform image segmentation. Although the DE optimization has been used in different fields, still there are no reports of its adoption in image matching.

In order to address these issues, we have proposed a differential evolution-based sample consensus algorithm (DESCA) to eliminate the outliers in the set of the correct matching candidates. The proposed method is very effective for the remote sensing optical images having affine geometric differences. The reasons of selecting the DE are as follows: DE gives better performance than the other optimization methods such as PSO and cooperative PSO variants and the number of control parameters in DE is very less [31]. The following contributions are incorporated in this paper:

1) DE optimization is introduced in image matching to eliminate the outliers and to identify the correct matches. Although the DE optimization has been utilized in different fields such as classification problems, computational system and image segmentation, still its adoption in image matching is not reported in the literature. In our proposed method, DE is combined with RANSAC to maximize the number of correct matching pairs.
2) In standard DE, the parameter vector $X$ is initialized randomly. However, a random initialization of $X$ fails to identify the correct matches in image matching as DE diverges because of the random selection of the values. Therefore, the initialization process of the $X$ is developed in this work so that better convergence can be achieved in image matching.

## II. PROPOSED METHOD

Fig. 1 shows the steps of the proposed method. At first, M-UR-SIFT [7] features are extracted from the input optical images. The main objective of this feature extraction algorithm is to provide uniformly distributed feature points. Then, feature matching is performed between the images and two sets of matching pairs are obtained. The first set of matching pairs is obtained by considering $d_{ratio} = 1$ (defined in section II-C) and the second set is obtained by

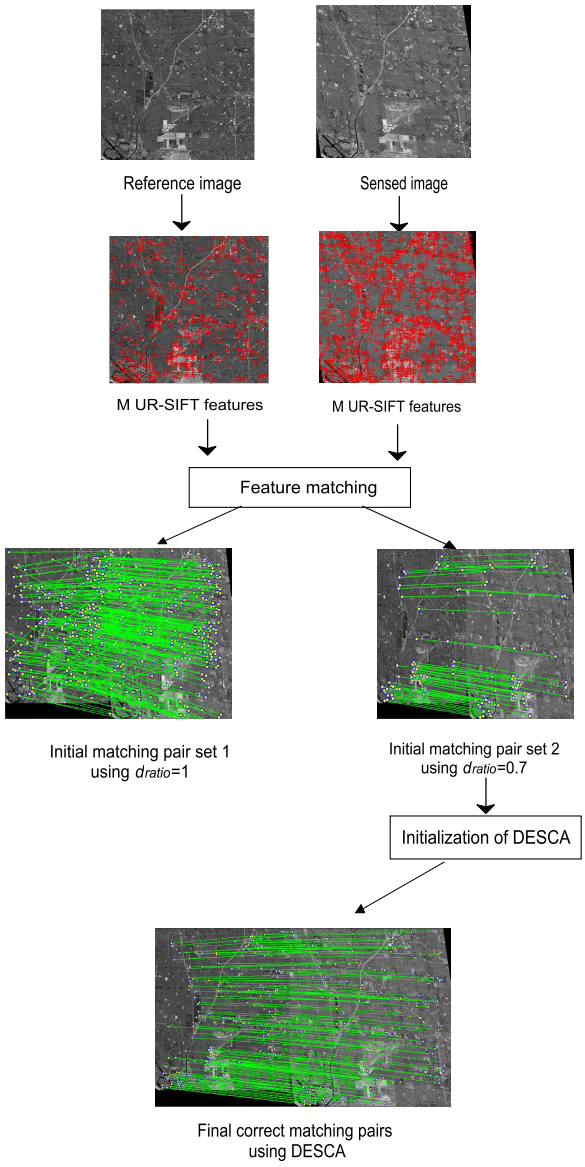


**FIGURE 1.** Flow chart of the proposed method.

selecting $d_{ratio} = 0.7$. As the second set of matching pairs is obtained by using lower value of $d_{ratio}$, it provides better correct matching rate (CMR) [CMR=number of correct matches/total matches]. So, this set of matching pair is utilized to initialize the DESCA algorithm. Finally, the DESCA algorithm identifies the correct matches between the input images using the first set of matching pairs.

### A. FEATURE EXTRACTION BY M-UR-SIFT ALGORITHM

In a previous research, we have developed a M-UR-SIFT algorithm [7] which is very effective to provide uniformly distributed features. Motivated by its feature extraction performance, it has been utilized to extract features in this proposed method. The feature extraction process of the M-UR-SIFT algorithm contains two steps: initial feature

extraction and final feature selection. In the initial feature extraction step, features are extracted from the Gaussian filtered images by considering a threshold value of 10% of the contrast range of the images. The entropy and contrast values are computed for these initial features. In the final selection step, a predefined number of features are selected from the initial features based on their entropy as well as contrast values and maintaining a specific distance between them. More detailed description of the M-UR-SIFT algorithm is available in [7].

### B. DE OPTIMIZATION

This section provides a brief idea of the DE Optimization. As the DE is a population based optimization, the population matrix can be given as

$$X_i^G = [x_{1,i}^G, x_{2,i}^G, x_{3,i}^G .., x_{D,i}^G] \tag{1}$$

where $X_i$ is known as genome/chromosome and $G$ denotes generation which represents individual updation.

#### 1) INITIALIZATION

In the standard DE optimization, the values of $X_i$ at the first generation (i.e. $G$=0) is chosen randomly within the search space.

#### 2) DIFFERENCE VECTOR MUTATION

In this step, a mutant vector $M_i^G$ is generated by using three randomly selected vectors ($X_{r_1}^G, X_{r_2}^G, X_{r_3}^G$ ) from $X_i^G$.

$$M_i^G = X_{r_1}^G + F(X_{r_2}^G - X_{r_3}^G) \tag{2}$$

where $F$ is the scale factor. The mutant vector $M_i^G$ is called as donor vector.

#### 3) CROSSOVER

In this step, the donor vector $M_i^G$ exchanges its components with the vector $X_i^G$ through binomial crossover to generate a trial vector $U_i^G$. This is performed in the following way:

$$U_{j,i}^G = \begin{cases} M_{j,i}^G, & \text{if } rand_{j,i}\,[0,1] \le C_r \text{ or } j = j_{rand}. \\ X_{j,i}^G, & \text{otherwise.} \end{cases} \tag{3}$$

where $C_r$ is the crossover rate.

#### 4) SELECTION

This step determines whether to select trail vector $U_i^G$ or $X_i^G$ for the next generation ($G$=$G$+1) based on following conditions:

$$X_i^{G+1} = \begin{cases} U_i^G, & \text{if } f(U_i^G) \ge f(X_i^G). \\ X_i^G, & \text{otherwise.} \end{cases} \tag{4}$$

### C. INITIALIZATION OF THE DESAC

The M-UR-SIFT features extracted from the input images are matched considering $d_{ratio}$=1 where $d_{ratio}$ is defined as the ratio between the distance of the nearest neighbor and that of the second nearest neighbor. The set of these matching pairs is represented as $\{(R_1,S_1),(R_2,S_2), \ldots .., (R_n,S_N)\}$. Another set of matching pairs is obtained by considering $d_{ratio} = t$ where $t < 1$. This set of matching pairs is represented as $\{(r_1,s_1),(r_2,s_2), \ldots .., (r_n,s_n)\}$. As this set is obtained by considering $t < 1$, it contains less number of outliers compared to the other set of matching pairs. This set is utilized to initialize the parameters of DESCA. An affine transformation model is selected as a transformation model in DESCA because this model can handle the geometric transformation differences of most of the optical images.

In our proposed method, the transformation parameters of the affine transformation model are considered as vector $X$. The objective function $f$ is considered as the number of matches satisfies the transformation model with a distance threshold value of 1 pixel. The standard DE optimization initializes the values of the vector $X$ randomly. However, as our proposed method utilizes the DE optimization to remove the outliers, the values of the vector $X$ can not be initialized randomly. The second set of matching pairs is used to find the initial values of $X$. As the set $\{(r_1,s_1),(r_2,s_2), \ldots .., (r_n,s_n)\}$ contains less number of outliers, these are eliminated one by one using $\text{RMSE}_{\text{LOO}}$ (root mean square error by leaving one out) parameter [38]. $\text{RMSE}_{\text{LOO}}$ is the calculated RMSE value of $M-1$ points from a set of $M$ points by excluding 1 point. The exclusion of the matching pair which gives the minimum RMSE is eliminated in every iteration until the $\text{RMSE}_{\text{LOO}}$ value becomes less than or equal to 1. Three number of pairs are selected randomly from the remaining matching pairs to determine the parameter values of the affine transformation and this is performed five times to get the population of the vector $X$. In this way, the vector $X$ initialized in our proposed method.

### D. DESCA FOR THE REMOVAL OF OUTLIERS

The main objective of the proposed DESCA is to update the values of $X$ such a way so that maximum number of correct matching pairs can be obtained while removing the outliers. In order to do that, the initialized vector $X$ is utilized to compute the donor vector $M$ using equation (2). Then, crossover is performed between $M$ and $X$ following the equation (3). After that, the vector $X$ is updated for the next iteration using the equation (4). The conditions of the equation (4) are checked by using the first set of matching pairs i.e. $\{(R_1,S_1),(R_2,S_2), \ldots .., (R_n,S_N)\}$. The number of matching pairs satisfies the transformation model of the vector $X$ and the vector $U$ are separately identified from the set $\{(R_1,S_1),(R_2,S_2), \ldots .., (R_n,S_N)\}$. Out of $X$ and $U$, the one which provides comparatively more matching pairs is selected as the transformation model for the next iteration. The steps followed in DESCA are provided in Algorithm 1.

The main advantages of the proposed method are as follows:

1) As the proposed DESCA algorithm finds the matching pairs by optimizing the parameters of the transformation model, it can provide more correct matching pairs.

**TABLE 1. Details of experimental data sets.**

| Set | Image | Sensor | Band | Size(pixels) | Resolution(m) | Date | Location |
|---|---|---|---|---|---|---|---|
| 1 | RI | Landsat ETM+ | 7 (2.09-2.35 $\mu$m) | 500×500 | 30 | 01/05/2000 | California |
| | SI | Landsat TM | 5 (1.55-1.75 $\mu$m) | 550×600 | 30 | 06/07/1992 | |
| 2 | RI | Landsat ETM+ | 2 (0.52 - 0.60 $\mu$m) | 600×600 | 30 | 05/10/2001 | Baltimore |
| | SI | Landsat TM | 7 (2.09-2.35 $\mu$m) | 550×600 | 30 | 16/05/1987 | |
| 3 | RI | IRS LISS-3 | 4 (0.77-0.86 $\mu$m) | 900×900 | 24 | 07/08/2017 | Toronto |
| | SI | Landsat ETM+ | 4 (0.77-0.90 $\mu$m) | 700×700 | 30 | 03/09/1999 | |
| 4 | RI | Landsat ETM+ | 8 (0.52-0.90 $\mu$m) | 900×900 | 15 | 01/05/2000 | California |
| | SI | IRS LISS-3 | 4 (0.77-0.86 $\mu$m) | 600×600 | 24 | 11/06/2018 | |
| 5 | RI | OrbView-3 | Pan (0.45-0.90 $\mu$m) | 1000×1000 | 1 | 13/06/2004 | Barcelona |
| | SI | OrbView-3 | Pan (0.45-0.90 $\mu$m) | 1000×1000 | 1 | 02/10/2005 | |
| 6 | RI | EO-ALI | 4 (0.84-0.89 $\mu$m) | 800×800 | 30 | 16/04/2010 | Chesapeake |
| | SI | Landsat TM | 7 (2.09-2.35 $\mu$m) | 800×800 | 30 | 30/07/1988 | |
| 7 | RI | IRS LISS-3 | 3 (0.62-0.68 $\mu$m) | 700×700 | 24 | 30/10/2017 | Cape Canaveral |
| | SI | EO-ALI | 5 (0.63-0.69 $\mu$m) | 500×500 | 30 | 09/06/2002 | |
| 8 | RI | IRS LISS-3 | 3 (0.62-0.68 $\mu$m) | 700×700 | 24 | 30/10/2017 | Cape Canaveral |
| | SI | Landsat TM | 7 (2.09-2.35 $\mu$m) | 550×550 | 30 | 24/04/1989 | |
| 9 | RI | Landsat ETM+ | 8 (0.52-0.90 $\mu$m) | 1000×1000 | 15 | 26/06/2000 | Campbell river |
| | SI | Landsat TM | 5 (1.55-1.75 $\mu$m) | 500×500 | 30 | 08/07/1989 | |

2) It can obtain better position accuracy (lesser RMSE) and higher mutual information (MI) values in optical image matching.

## III. EXPERIMENTAL RESULTS

### A. SELECTED DATA SETS

Nine sets of optical image pairs are (Available: http://earthexplorer.usgs.gov) selected to verify the performance of the proposed method. Fig. 2 shows the images of the eight data sets and the detailed information of these sets is provided in Table 1. In this table, RI and SI represent reference image and sensed image respectively.

### B. QUANTITATIVE ASSESSMENT PARAMETERS

1) Number of correct matching pairs (NCMP): It is defined as the number of correctly matching pairs identified in an image pair by a matching algorithm. In order to identify the correct matching pairs, 30 uniformly distributed tie points are selected from the input images. Then, these tie points are applied in an affine transformation model to calculate the transformation between the input images. A matching pair satisfies this estimated transformation with a distance threshold value of 1 pixel is considered as a correct matching pair.
2) Root mean square error (RMSE): In order to find RMSE value, the residual errors of the correct matching pairs are calculated first. The root means square of these residual errors is considered as RMSE.
3) Mutual information (MI): MI represents the statistical dependance between the input images [5].

### C. SELECTION OF PARAMETERS

In the initialization process of the DESCA, the set $\{(r_1,s_1),(r_2,s_2),\ldots..,(r_n,s_n)\}$ is obtained by considering the value of $t$=0.7 (i.e. $d_{ratio}$=0.7). According to [24], this value of $t$ provides better CMR with sufficient correct matching

**Algorithm 1** Differential Evolution-based Sample Consensus Algorithm (DESCA)

**Input**:
- $X$ : Initialized transformation model parameter vector.
- $\{(R_1,S_1),(R_2,S_2),\ldots..,(R_n,S_N)\}$: Set of initial matching pairs.

**Output**:
- $X_f$ : Final transformation model parameter vector.
- $P_f$ : Final matching pairs

(1) **for** $G = 0 : N$
(2) Update a donor vector $M^G$ by using three randomly selected vectors from $X^G$ based on equation 2.
(3) Update a trial vector $U^G$ using equation 3.
(4) Identify the matching pairs $(R_X, S_X)$ from $\{(R_1,S_1),(R_2,S_2),\ldots..,(R_n,S_N)\}$ which satisfies the transformation model parameter of the vector $X^G$.
(5) $N_1 = \text{size}\{(R_X, S_X)\}$
(6) Identify the matching pairs $(R_U, S_U)$ from $\{(R_1,S_1),(R_2,S_2),\ldots..,(R_n,S_N)\}$ which satisfies the transformation model parameter of the vector $U^G$.
(7) $N_2 = \text{size}\{(R_U, S_U)\}$
(8) **if** $N_1 > N_2$ **do**
(9) $X^{G+1} = X^G$.
(10) $P_f = (R_X, S_X)$.
(11) **else**
(12) $X^{G+1} = U^G$.
(13) $P_f = (R_U, S_U)$
(14) **end if**
(15) **end for**
(16) $X_f = X^N$

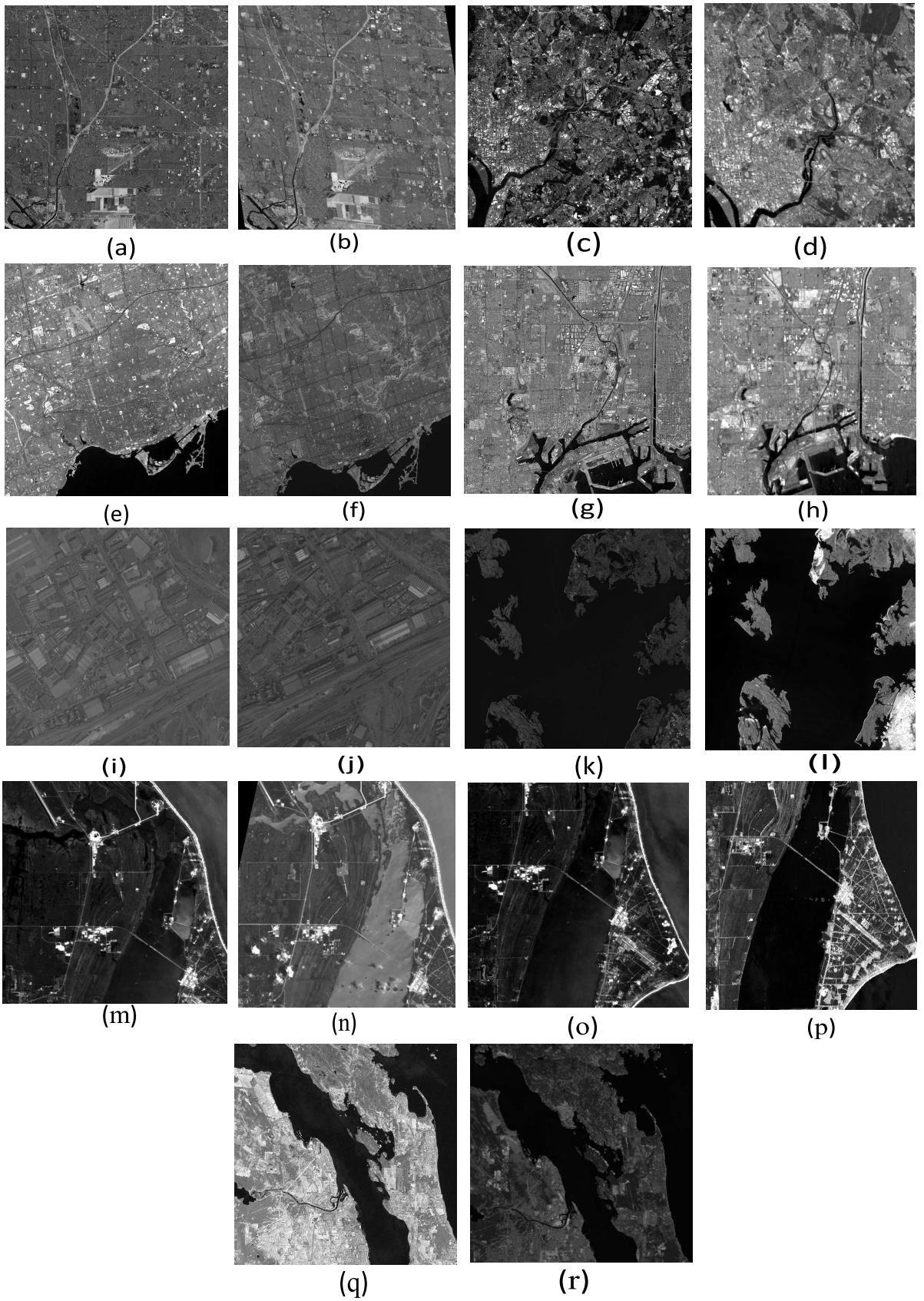


**FIGURE 2.** Selected data sets. (a) and (b) are set 1. (c) and (d) are set 2. (e) and (f) are set 3. (g) and (h) are set 4. (i) and (j) are set 5. (k) and (l) are set 6. (m) and (f) are set 7. (o) and (p) are set 8. (q) and (r) are set 9.

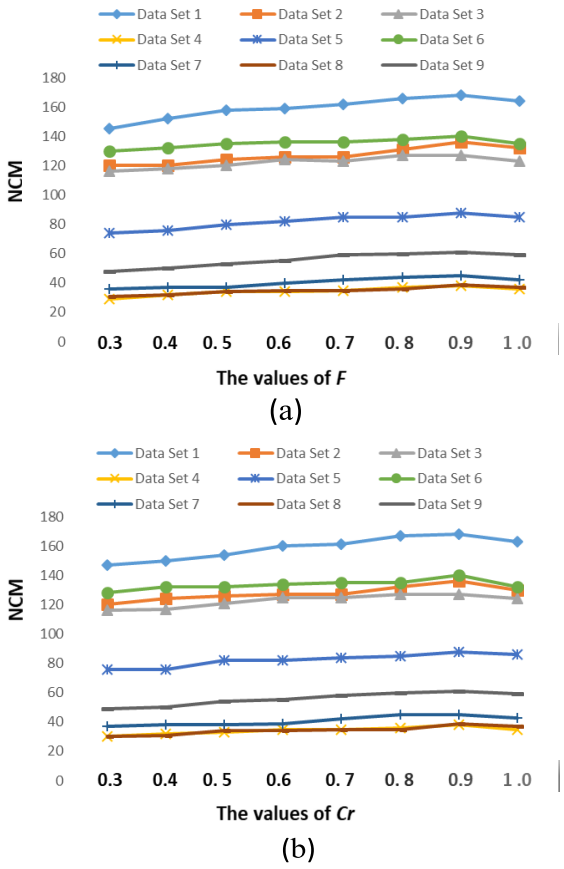


**FIGURE 3.** (a) Effect of $F$ on the NCMP and (b) effect of $C_r$ on NCMP for the different data sets.

pairs. A large value of $t$ reduces the CMR value which makes the initialization erroneous whereas a very small value of $t$ provides insufficient correct matching pairs. Initialisation of the DESCA is not recommended with insufficient matching pairs. The values of $F$, $C_r$ are set by analysing the experiment results of the selected data sets. Fig. 3(a) and 3(b) show the effect of $F$, $C_r$ parameter's values on the NCMP. From these figures, it can be observed that initially, the NCMP values increase with the increase of the values of the parameters and maximum value of NCMP is obtained at 0.9. However, after 0.9, the values again decrease. Considering these effects, the values of $F$ and $C_r$ are set to 0.9. According to the standard DE optimization [31], the value $G$ is decided as 200.

### D. ANALYSIS OF MATCHING RESULTS

In order to show the effectiveness of the proposed method, it is compared with the other seven state-of-the-art methods: ORB [18], SURF [17], DM [22], DOC [25], FSC [24], MGEO [27], and A-RKEM [10]. In each of the methods, the M-UR-SIFT algorithm is utilized for feature extraction except A-RKEM.

The correct matching pairs obtained by the ORB, SURF, DM, DOC, FSC, A-RKEM, and the proposed DESCA algorithms for the data set 1, data set 2, data set 3 and data set 4 are shown in Fig. 4, Fig. 5, Fig. 6, and Fig. 7, respectively. From these figures, it can be observed that the FSC obtained comparatively more correct matching pairs than the SURF, ORB, DM, DOC, and A-RKEM algorithms. However, the best matching results are obtained by the proposed DESCA algorithm as it provides more correct matching pairs than other methods.

Table 2 and Table 3 provide the quantitative assessment results of the SURF, ORB, DM, DOC, FSC, MGEO,

**TABLE 2.** Quantitative Results of ORB [18], SURF [17], DM [22], DOC [25], FSC [24], MGEO [27], A-RKEM [10] and DESCA.

| Data Set | Method | NCMP | RMSE | MI |
|---|---|---|---|---|
| 1 | ORB [18] | 8 | 0.991 | 0.897 |
| | SURF [17] | 48 | 0.931 | 0.906 |
| | DM [22] | 81 | 0.881 | 0.918 |
| | DOC [25] | 110 | 0.803 | 0.937 |
| | FSC [24] | 131 | 0.785 | 0.945 |
| | MGEO [27] | 121 | 0.792 | 0.942 |
| | A-RKEM [10] | 116 | 0.796 | 0.941 |
| | **DESCA** | 168 | 0.730 | 0.959 |
| 2 | ORB [18] | 9 | 0.942 | 0.616 |
| | SURF [17] | 59 | 0.764 | 0.628 |
| | DM [22] | 78 | 0.725 | 0.632 |
| | DOC [25] | 92 | 0.706 | 0.641 |
| | FSC [24] | 112 | 0.688 | 0.650 |
| | MGEO [27] | 101 | 0.692 | 0.648 |
| | A-RKEM [10] | 96 | 0.700 | 0.645 |
| | **DESCA** | 136 | 0.675 | 0.658 |
| 3 | ORB [18] | 17 | 0.943 | 0.815 |
| | SURF [17] | 39 | 0.906 | 0.826 |
| | DM [22] | 66 | 0.887 | 0.830 |
| | DOC [25] | 72 | 0.860 | 0.836 |
| | FSC [24] | 88 | 0.848 | 0.843 |
| | MGEO [27] | 82 | 0.852 | 0.841 |
| | A-RKEM [10] | 77 | 0.857 | 0.838 |
| | **DESCA** | 127 | 0.791 | 0.862 |
| 4 | ORB [18] | 6 | 0.990 | 0.402 |
| | SURF [17] | 5 | 0.992 | 0.401 |
| | DM [22] | 12 | 0.982 | 0.403 |
| | DOC [25] | 16 | 0.973 | 0.412 |
| | FSC [24] | 24 | 0.965 | 0.424 |
| | MGEO | 20 | 0.970 | 0.418 |
| | A-RKEM [10] | 18 | 0.972 | 0.415 |
| | **DESCA** | 38 | 0.936 | 0.437 |
| 5 | ORB [18] | 22 | 0.999 | 0.286 |
| | SURF [17] | 19 | 1.000 | 0.285 |
| | DM [22] | 46 | 0.995 | 0.287 |
| | DOC [25] | 52 | 0.986 | 0.288 |
| | FSC [24] | 60 | 0.978 | 0.293 |
| | MGEO [27] | 57 | 0.982 | 0.290 |
| | A-RKEM [10] | 55 | 0.984 | 0.289 |
| | **DESCA** | 88 | 0.959 | 0.302 |

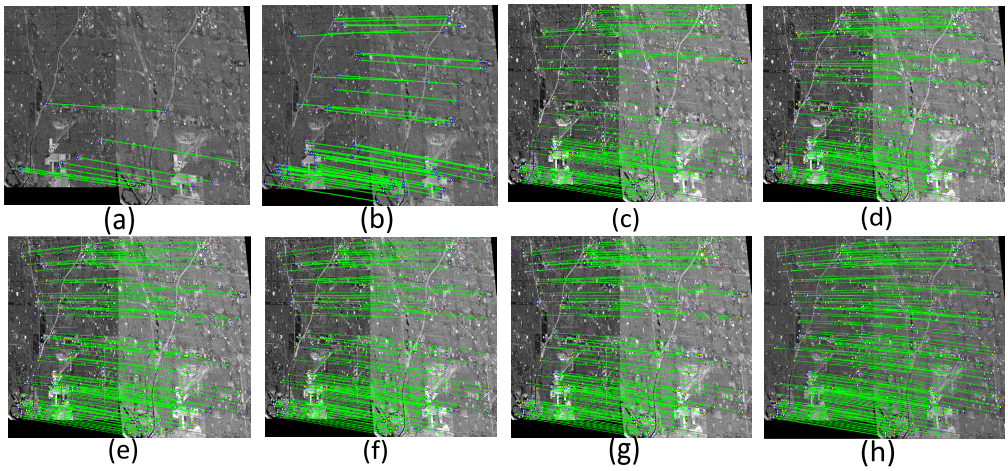


**FIGURE 4.** Correct matching pairs for Data Set 1. (a) ORB. (b) SURF. (c) DM. (d) DOC. (e) FSC. (f) MGEO. (g) A-RKEM. (h) DESCA.

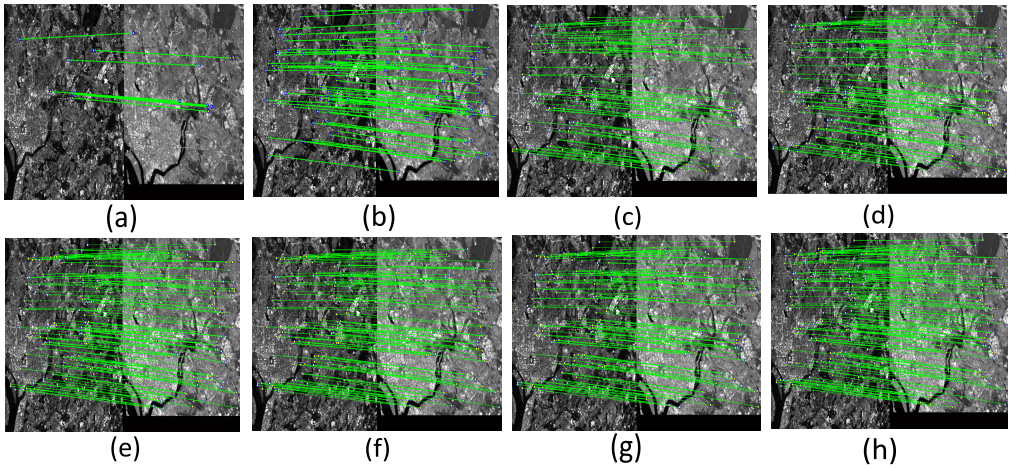


**FIGURE 5.** Correct matching pairs for Data Set 2. (a) ORB. (b) SURF. (c) DM. (d) DOC. (e) FSC. (f) MGEO. (g) A-RKEM. (h) DESCA.

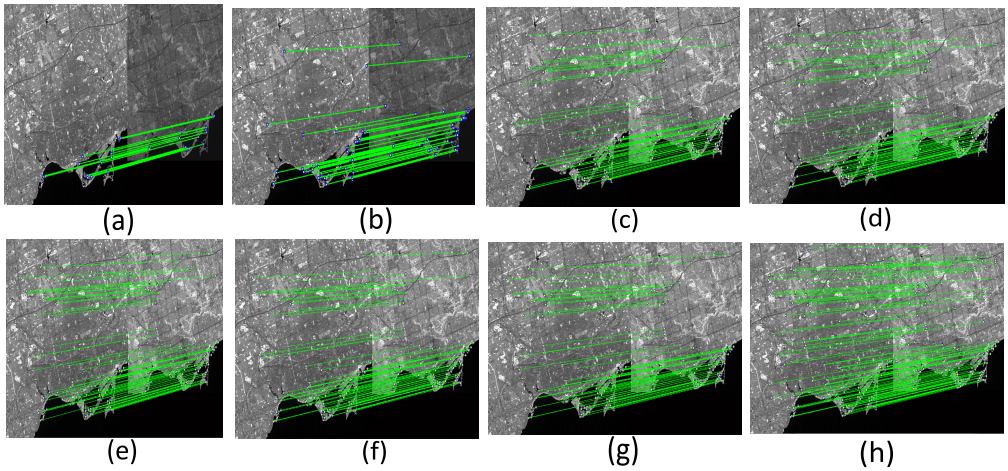


**FIGURE 6.** Correct matching pairs for Data Set 3.(a) ORB. (b) SURF. (c) DM. (d) DOC. (e) FSC. (f) MGEO. (g) A-RKEM. (h) DESCA.

A-RKEM and the proposed DESCA algorithms. This table shows that the FSC algorithm obtains more NCMP values than the SURF, ORB, DM, DOC, A-RKEM and MGEO algorithms. However, the highest NCMP values are obtained by the proposed DESCA algorithm and these values are significantly better in DESCA compared to the other

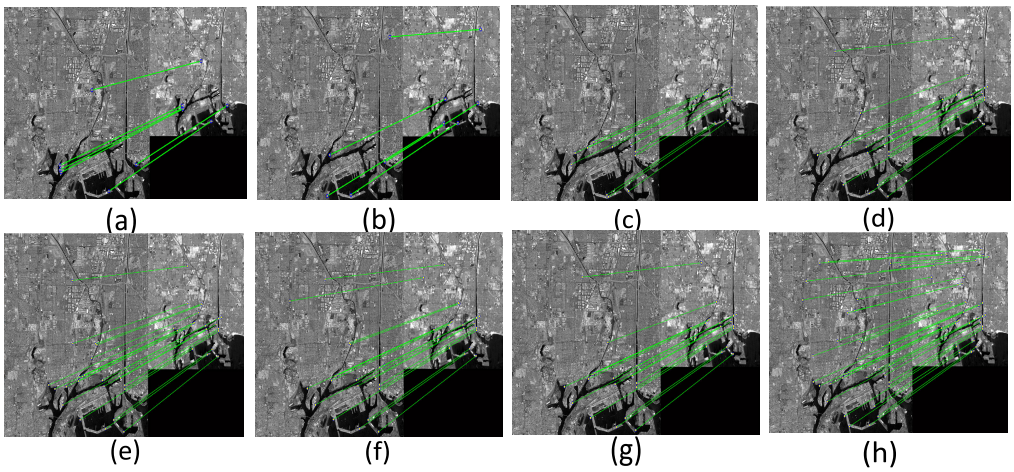


**FIGURE 7.** Correct matching pairs for Data Set 4. (a) ORB. (b) SURF. (c) DM. (d) DOC. (e) FSC. (f) MGEO. (g) A-RKEM. (h) DESCA.

**TABLE 3.** Quantitative Results of ORB [18], SURF [17], DM [22], DOC [25], FSC [24], MGEO [27], A-RKEM [10] and DESCA.

| Data Set | Method | NCMP | RMSE | MI |
|---|---|---|---|---|
| 6 | ORB [18] | 18 | 0.975 | 0.589 |
| | SURF [17] | - | - | - |
| | DM [22] | 76 | 0.875 | 0.504 |
| | DOC [25] | 89 | 0.842 | 0.508 |
| | FSC [24] | 122 | 0.823 | 0.512 |
| | MGEO [27] | 109 | 0.830 | 0.510 |
| | A-RKEM [10] | 102 | 0.834 | 0.509 |
| | **DESCA** | 140 | 0.800 | 0.519 |
| 7 | ORB [18] | 11 | 0.997 | 0.245 |
| | SURF [17] | 18 | 0.990 | 0.246 |
| | DM [22] | 20 | 0.988 | 0.247 |
| | DOC [25] | 22 | 0.967 | 0.249 |
| | FSC [24] | 34 | 0.924 | 0.254 |
| | MGEO [27] | 28 | 0.943 | 0.252 |
| | A-RKEM [10] | 26 | 0.950 | 0.250 |
| | **DESCA** | 45 | 0.901 | 0.258 |
| 8 | ORB [18] | - | - | - |
| | SURF [17] | - | - | - |
| | DM [22] | 18 | 0.990 | 0.267 |
| | DOC [25] | 22 | 0.973 | 0.270 |
| | FSC [24] | 28 | 0.961 | 0.275 |
| | MGEO [27] | 25 | 0.965 | 0.273 |
| | A-RKEM [10] | 23 | 0.970 | 0.271 |
| | **DESCA** | 39 | 0.947 | 0.279 |
| 9 | ORB [18] | - | - | - |
| | SURF [17] | 5 | 0.996 | 0.474 |
| | DM [22] | 20 | 0.966 | 0.482 |
| | DOC [25] | 26 | 0.952 | 0.484 |
| | FSC [24] | 46 | 0.901 | 0.495 |
| | MGEO [27] | 34 | 0.946 | 0.487 |
| | A-RKEM [10] | 30 | 0.949 | 0.486 |
| | **DESCA** | 61 | 0.856 | 0.502 |

methods. If parameter vector X is initialized randomly in DESCA, then no correct matches are obtained between the images as DE divergences due to the random initialization. However, the DESCA gives 168, 136, 127, 38, 88, 140, 45, 39, and 61 correct matches for data set 1, 2, 3, 4, 5, 6, 7, 8, and 9 respectively when the proposed initialization method is followed.

The SURF algorithm fails to find correct matching pairs for data set 6 and 8. On the other hand, ORB gives no matching pairs for data set 8 and 9. As SURF algorithm is less robust compared to SIFT, it gives comparatively less correct matches than DM, DOC, FSC, MGEO, A-RKEM, and DESCA which are based on SIFT. The ORB uses binary features which are sensitive to significant intensity variations. As results, ORB gives less matching pairs. The DM algorithm eliminates the outliers by maintaining a nearest neighbor distance ratio value of 0.8 for both the input image features. This criterion removes many correct matching pairs and as a result, it gives less NCMP values. The DOC algorithm eliminates the incorrect matching pairs by checking their dominant orientation. However, the dominant orientation of the SIFT features is not consistent for all the features [39]. In case of MGEO also, the correct matches are selected by using gradient orientation which does not remain consistent in many cases. As a result, these methods loose many correct matching pairs. As the A-RKEM algorithm uses NNDR criterion to remove the outliers, it loosed many correct matches. Although the FSC algorithm obtains more NCMP values than DM and DOC, still it is less than the proposed DESCA. The reason is that the DESCA finds the matching pairs by optimizing the parameter of transformation model whereas FSC uses a sample corresponding set. As the proposed DESCA obtains better NCMP values, the position accuracy is higher in this method. Therefore, it provides better RMSE and MI values for all the data sets compared to other methods.

### E. DISCUSSION

Experiment on different sets of data sets shows that the proposed DESCA gives more correct matching pairs and

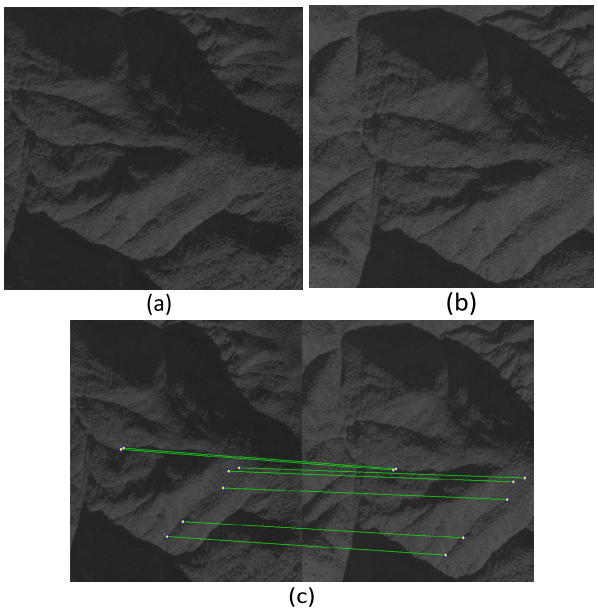


**FIGURE 8.** Limitation of the proposed method. (a) and (b) are input optical images. (c) Matching pairs obtained by DESCA algorithm.

better MI values. In addition, it gives better position accuracy as the obtained RMSE values are less. The proposed method is applicable for the remote sensing optical images having translation, rotation, scaling, and shearing differences. The introduction of DE optimization in image matching and the initialization process of the DE optimization are the novelties of the proposed method. Although the proposed DESCA algorithm works nicely for the remote sensing optical images with affine geometric differences, it fails to provide satisfactory results for the mountain images which contain local geometric differences caused by terrain relief. Fig. 8(a) and 8(b) show two images captured by OrbView-3 sensor (resolution 1 meter) covering the mountain area of Kathmandu, Nepal. The size of the images is $800 \times 800$ pixels and these are captured on October 11, 2005. Fig. 8(c) shows the matching pairs obtained by DESCA algorithm for these input images. From this figure, it can be observed that the number of correct matching pairs is very less. As the mountain images contain local distortions due to terrain relief, the global affine model used in DESCA algorithm can not properly handle these local geometric differences. Therefore, the proposed method obtains less correct matches for this data set.

## IV. CONCLUSION

In this paper, a DESCA algorithm is proposed to match the remote sensing optical images having affine geometric differences. At first, a M-UR-SIFT algorithm is utilized for feature extraction as well as feature matching between the input images. Two sets of matching pairs are obtained in the feature matching process. The first set is used for the initialization of the proposed DESCA algorithm. The second set is utilized to find the correct matching pairs using the DESCA algorithm. Experiments on different sets of high and medium resolution optical image pairs shows that the developed scheme can provide better NCMP and MI values than the existing well-known outlier removal algorithms. In addition, it can achieve precise accuracy in optical image matching. Although the proposed method performs nicely for most of the remote sensing optical images, still provides less number of correct matching pairs for mountain images which contain local deformations. In order to match such images, the polynomial model can be used as a transformation model in the DESCA algorithm which is one of our future works. In addition, DE optimization will be used along with an appropriate transfer model for 3D point cloud registration where the optimization process plays a critical role [40], [41].

## REFERENCES

[1] A. Sedaghat, M. Mokhtarzade, and H. Ebadi, "Uniform robust scale-invariant feature matching for optical remote sensing images," *IEEE Trans. Geosci. Remote Sens.*, vol. 49, no. 11, pp. 4516–4527, Nov. 2011.

[2] D. Hong, B. Zhang, X. Li, Y. Li, C. Li, J. Yao, N. Yokoya, H. Li, P. Ghamisi, X. Jia, A. Plaza, P. Gamba, J. A. Benediktsson, and J. Chanussot, "SpectralGPT: Spectral remote sensing foundation model," *IEEE Trans. Pattern Anal. Mach. Intell.*, early access, Apr. 3, 2024, doi: 10.1109/TPAMI.2024.3362475.

[3] D. Hong, B. Zhang, H. Li, Y. Li, J. Yao, C. Li, M. Werner, J. Chanussot, A. Zipf, and X. X. Zhu, "Cross-city matters: A multimodal remote sensing benchmark dataset for cross-city semantic segmentation using high-resolution domain adaptation networks," *Remote Sens. Environ.*, vol. 299, Dec. 2023, Art. no. 113856.

[4] D. Hong, J. Yao, C. Li, D. Meng, N. Yokoya, and J. Chanussot, "Decoupled-and-coupled networks: Self-supervised hyperspectral image super-resolution with subpixel fusion," *IEEE Trans. Geosci. Remote Sens.*, vol. 61, 2023, Art. no. 5527812.

[5] S. Paul and U. C. Pati, "High-resolution optical-to-SAR image registration using mutual information and SPSA optimisation," *IET Image Process.*, vol. 15, no. 6, pp. 1319–1331, May 2021.

[6] D. G. Lowe, "Distinctive image features from scale-invariant keypoints," *Int. J. Comput. Vis.*, vol. 60, no. 2, pp. 91–110, Nov. 2004.

[7] S. Paul and U. C. Pati, "Remote sensing optical image registration using modified uniform robust SIFT," *IEEE Geosci. Remote Sens. Lett.*, vol. 13, no. 9, pp. 1300–1304, Sep. 2016.

[8] Y. Li, W. Qiao, H. Jin, J. Jing, and C. Fan, "Reliable and fast mapping of keypoints on large-size remote sensing images by use of multiresolution and global information," *IEEE Geosci. Remote Sens. Lett.*, vol. 12, no. 9, pp. 1983–1987, Sep. 2015.

[9] I.-H. Lee and T.-S. Choi, "Accurate registration using adaptive block processing for multispectral images," *IEEE Trans. Circuits Syst. Video Technol.*, vol. 23, no. 9, pp. 1491–1501, Sep. 2013.

[10] Z. Hossein-Nejad, H. Agahi, and A. Mahmoodzadeh, "Image matching based on the adaptive redundant keypoint elimination method in the SIFT algorithm," *Pattern Anal. Appl.*, vol. 24, no. 2, pp. 669–683, May 2021.

[11] A. Sedaghat and H. Ebadi, "Distinctive order based self-similarity descriptor for multi-sensor remote sensing image matching," *ISPRS J. Photogramm. Remote Sens.*, vol. 108, pp. 62–71, Oct. 2015.

[12] Y. Ye and J. Shan, "A local descriptor based registration method for multispectral remote sensing images with non-linear intensity differences," *ISPRS J. Photogramm. Remote Sens.*, vol. 90, pp. 83–95, Apr. 2014.

[13] E. Shechtman and M. Irani, "Matching local self-similarities across images and videos," in *Proc. IEEE Conf. Comput. Vis. Pattern Recognit.*, Jun. 2007, pp. 1–8.

[14] Y. Ye, M. Wang, S. Hao, and Q. Zhu, "A novel keypoint detector combining corners and blobs for remote sensing image registration," *IEEE Geosci. Remote Sens. Lett.*, vol. 18, no. 3, pp. 451–455, Mar. 2021.

[15] J. Jiang and X. Shi, "A robust point-matching algorithm based on integrated spatial structure constraint for remote sensing image registration," *IEEE Geosci. Remote Sens. Lett.*, vol. 13, no. 11, pp. 1716–1720, Nov. 2016.
[16] S. Paul, D. Udaysankar, Y. Naidu, and Y. Reddy, "Uniform distribution of multiple features for remote sensing optical image matching," in *Proc. 10th Int. Conf. Emerg. Trends Eng. Technol.-Signal Inf. Process.*, Apr. 2022, pp. 1–5.
[17] H. Bay, A. Ess, T. Tuytelaars, and L. Van Gool, "Speeded-up robust features (SURF)," *Comput. Vis. Image Understand.*, vol. 110, no. 3, pp. 346–359, Jun. 2008.
[18] E. Rublee, V. Rabaud, K. Konolige, and G. Bradski, "ORB: An efficient alternative to SIFT or SURF," in *Proc. Int. Conf. Comput. Vis.*, Nov. 2011, pp. 2564–2571.
[19] B. Zhu, C. Yang, J. Dai, J. Fan, Y. Qin, and Y. Ye, "$R_2FD_2$: Fast and robust matching of multimodal remote sensing images via repeatable feature detector and rotation-invariant feature descriptor," *IEEE Trans. Geosci. Remote Sens.*, vol. 61, 2023, Art. no. 5606115.
[20] L. Zhou, Y. Ye, T. Tang, K. Nan, and Y. Qin, "Robust matching for SAR and optical images using multiscale convolutional gradient features," *IEEE Geosci. Remote Sens. Lett.*, vol. 19, pp. 1–5, 2022.
[21] Y. Ye, B. Zhu, T. Tang, C. Yang, Q. Xu, and G. Zhang, "A robust multimodal remote sensing image registration method and system using steerable filters with first- and second-order gradients," *ISPRS J. Photogramm. Remote Sens.*, vol. 188, pp. 331–350, Jun. 2022.
[22] S. Wang, H. You, and K. Fu, "BFSIFT: A novel method to find feature matches for SAR image registration," *IEEE Geosci. Remote Sens. Lett.*, vol. 9, no. 4, pp. 649–653, Jul. 2012.
[23] M. A. Fischler and R. Bolles, "Random sample consensus: A paradigm for model fitting with applications to image analysis and automated cartography," *Commun. ACM*, vol. 24, no. 6, pp. 381–395, 1981.
[24] Y. Wu, W. Ma, M. Gong, L. Su, and L. Jiao, "A novel point-matching algorithm based on fast sample consensus for image registration," *IEEE Geosci. Remote Sens. Lett.*, vol. 12, no. 1, pp. 43–47, Jan. 2015.
[25] F. Wang, H. You, and X. Fu, "Adapted anisotropic Gaussian SIFT matching strategy for SAR registration," *IEEE Geosci. Remote Sens. Lett.*, vol. 12, no. 1, pp. 160–164, Jan. 2015.
[26] B. Kupfer, N. S. Netanyahu, and I. Shimshoni, "An efficient SIFT-based mode-seeking algorithm for sub-pixel registration of remotely sensed images," *IEEE Geosci. Remote Sens. Lett.*, vol. 12, no. 2, pp. 379–383, Feb. 2015.
[27] Q. Wu and S. Zhu, "Multispectral image matching method based on histogram of maximum gradient and edge orientation," *IEEE Geosci. Remote Sens. Lett.*, vol. 19, pp. 1–5, 2022.
[28] S. Paul, Y. Naidu, and Y. Reddy, "An efficient SIFT-based matching algorithm for optical remote sensing images," *Remote Sens. Lett.*, vol. 13, no. 11, pp. 1069–1079, Sep. 2022.
[29] W. Ma, Z. Wen, Y. Wu, L. Jiao, M. Gong, Y. Zheng, and L. Liu, "Remote sensing image registration with modified SIFT and enhanced feature matching," *IEEE Geosci. Remote Sens. Lett.*, vol. 14, no. 1, pp. 3–7, Jan. 2017.
[30] Y. Wu, Q. Miao, W. Ma, M. Gong, and S. Wang, "PSOSAC: Particle swarm optimization sample consensus algorithm for remote sensing image registration," *IEEE Geosci. Remote Sens. Lett.*, vol. 15, no. 2, pp. 242–246, Feb. 2018.
[31] S. Das and P. N. Suganthan, "Differential evolution: A survey of the state-of-the-art," *IEEE Trans. Evol. Comput.*, vol. 15, no. 1, pp. 4–31, Feb. 2011.
[32] M. F. Ahmad, N. A. M. Isa, W. H. Lim, and K. M. Ang, "Differential evolution: A recent review based on state-of-the-art works," *Alexandria Eng. J.*, vol. 61, no. 5, pp. 3831–3872, May 2022.
[33] Y. Zhang, D.-W. Gong, X.-Z. Gao, T. Tian, and X.-Y. Sun, "Binary differential evolution with self-learning for multi-objective feature selection," *Inf. Sci.*, vol. 507, pp. 67–85, Jan. 2020.
[34] T. Marcic, B. Stumberger, and G. Stumberger, "Differential-evolution-based parameter identification of a line-start IPM synchronous motor," *IEEE Trans. Ind. Electron.*, vol. 61, no. 11, pp. 5921–5929, Nov. 2014.
[35] A. Céspedes-Mota, G. Castañón, A. F. Martínez-Herrera, L. E. Cárdenas-Barrón, and A. M. Sarmiento, "Differential evolution algorithm applied to wireless sensor distribution on different geometric shapes with area and energy optimization," *J. Netw. Comput. Appl.*, vol. 119, pp. 14–23, Oct. 2018.
[36] A. LaTorre, M. T. Kwong, J. A. García-Grajales, R. Shi, A. Jérusalem, and J.-M. Peña, "Model calibration using a parallel differential evolution algorithm in computational neuroscience: Simulation of stretch induced nerve deficit," *J. Comput. Sci.*, vol. 39, Jan. 2020, Art. no. 101053.
[37] S. Sarkar and S. Das, "Multilevel image thresholding based on 2D histogram and maximum Tsallis entropy—A differential evolution approach," *IEEE Trans. Image Process.*, vol. 22, no. 12, pp. 4788–4797, Dec. 2013.
[38] H. Goncalves, J. A. Goncalves, and L. Corte-Real, "Measures for an objective evaluation of the geometric correction process quality," *IEEE Geosci. Remote Sens. Lett.*, vol. 6, no. 2, pp. 292–296, Apr. 2009.
[39] B. Fan, C. Huo, C. Pan, and Q. Kong, "Registration of optical and SAR satellite images by exploring the spatial relationship of the improved SIFT," *IEEE Geosci. Remote Sens. Lett.*, vol. 10, no. 4, pp. 657–661, Jul. 2013.
[40] Y. Wu, H. Ding, M. Gong, A. K. Qin, W. Ma, Q. Miao, and K. C. Tan, "Evolutionary multiform optimization with two-stage bidirectional knowledge transfer strategy for point cloud registration," *IEEE Trans. Evol. Comput.*, vol. 28, no. 1, pp. 62–76, Feb. 2024.
[41] Y. Wu, Y. Liu, M. Gong, P. Gong, H. Li, Z. Tang, Q. Miao, and W. Ma, "Multi-view point cloud registration based on evolutionary multitasking with bi-channel knowledge sharing mechanism," *IEEE Trans. Emerg. Topics Comput. Intell.*, vol. 7, no. 2, pp. 357–374, Apr. 2023.

**SOURABH PAUL** received the B.E. degree in electronics and telecommunication engineering from Tripura Institute of Technology, Tripura, India, in 2011, the M.Tech. degree in electronics and communication engineering from the National Institute of Technology, Agartala, India, in 2014, and the Ph.D. degree in electronics and communication engineering from the National Institute of Technology, Rourkela, India, in 2019. Currently, he is an Assistant Professor (Senior) with the School of Electronics Engineering (SENSE), Vellore Institute of Technology (VIT), Chennai. He has the working experience of nearly ten years in research and teaching field. He has authored or coauthored a number of IEEE GEOSCIENCE AND REMOTE SENSING LETTERS, IEEE JOURNAL OF SELECTED TOPICS IN APPLIED EARTH OBSERVATIONS AND REMOTE SENSING, and other research papers on remote sensing image processing. His research interests include image registration, image matching, remote sensing image processing, and edge detection.

**RAVI TIWARI** received the B.E. degree in electronics and communication discipline from LNCTS, Bhopal, India, in 2011, and the M.Tech. and Ph.D. degrees in electronics and communication engineering from the National Institute of Technology, Rourkela, India, in 2014 and 2019, respectively. He has nearly ten years of experience in the field of teaching and research. He was an Assistant Professor with the Department of Electronics, G. H. Raisoni University, Nagpur. He was also a Senior Assistant Professor with the Department of Electronics and Communication, Madanapalle Institute of Technology and Science (MITS), Madanapalle, Andhra Pradesh, from May 2019 to Jan 2022. Since January 2022, he has been a Senior Assistant Professor with the Schools of Electronics Engineering (SENSE), Vellore Institute of Technology (VIT), Chennai, India. He has authored a number of reputed journals, such as IEEE TRANSACTION, IEEE Letters, and Wiley Transactions. His research interests include statistical signal processing, wireless communication, and information theory.

**AMIT KUMAR RAHUL** received the B.Sc., M.Sc., and B.Ed. degrees in mathematics from Dr. Ram Manohar Lohiya Avadh University, Ayodhya, Faizabad, Uttar Pradesh, in 2010, 2013, and 2014, respectively, and the Ph.D. degree in mathematics and computing from the Indian School of Mines, Indian Institute of Technology, Dhanbad, Jharkhand, India, in 2021. Currently, he is an Assistant Professor with the School of Advanced Sciences (SAS), Vellore Institute of Technology (VIT), Chennai. He has nearly six years of research experience and two years of teaching experience. He has authored or coauthored a number of journals for Elsevier, Springer, and Sage. His research interests include tribology, fluid film lubrication, non-newtonian lubricants, squeeze film flows, and nonlinear partial differential equations.

**MANOJ KUMAR SINGH** received the B.Sc. degree in mathematics, physics, and chemistry from Veer Bahadur Singh Purvanchal University, Jaunpur, India, in 2010, the M.Sc. degree in mathematics from Banaras Hindu University (Central University), Varanasi, India, and the Ph.D. degree in mathematics from IIT Dhanbad, in 2019. He was an Assistant Professor with the Department of Mathematics, Madanapalle Institute of Technology and Science (MITS), Madanapalle, Andhra Pradesh, from April 2019 to April 2022. Currently, he is an Assistant Professor (Grade-2) with the School of Advances Sciences (SAS), Vellore Institute of Technology (VIT), Chennai. He has the working experience of nearly nine years in research and teaching field. He has authored or coauthored in many research papers which have been published in many reputed journals. His research interest includes propagation of elastic waves in solids.

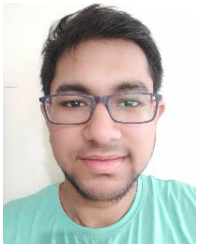

**PRATHAM GUPTA** is currently pursuing the bachelor's degree with the Computer Science and Engineering Program, Vellore Institute of Technology. As a undergraduate student, he exhibits a deep passion for the fields of image matching, image registration, machine learning, and artificial intelligence. Notably, by publishing a number of conference paper, he has made a significant academic contribution that highlights his commitment to furthering knowledge in his field of expertise. In his pursuit of knowledge, he continues to investigate the complex nexus between computer science, artificial intelligence, and machine learning.